Archives of Civil and Mechanical Engineering (2024) 24:200
https://doi.org/10.1007/s43452-024-00990-x

ORIGINAL ARTICLE

Engineering and microstructural properties of environmentally friendly alkali-activated composites containing clinker aggregate: heat-curing regime and elevated-temperature effect

Barış Bayrak[1] · Süleyman İpek[2] · Haluk Görkem Alcan[1] · Gökhan Kaplan[3] · Abdulkadir Cüneyt Aydın[3] · Erhan Güneyisi[4]

Received: 5 October 2023 / Revised: 24 May 2024 / Accepted: 5 June 2024 / Published online: 16 July 2024
© The Author(s) 2024

Abstract

The common wisdom in the literature about clinker aggregate (CA) is that it improves the performance properties of mortar or concrete to some extent. The current study, in this context, investigated the physical characteristics and mechanical performances of alkali-activated composites (AACs) made entirely with CA. The CA was used in three particle sizes of 0–2 mm (named No.10), 2–4 mm (named No.5), and 4–8 mm (named medium). To examine the impact of the fine CA-size fraction on the characteristics of AAC, No.10 CA was partially replaced by No.5 CA up to 50%, while the content of the medium CA was kept constant in all AAC mixtures. Moreover, to evaluate the influence of the 8-h curing temperature on the performance of the AACs, different temperature-based curing strategies (ambient, 45, and 75 °C) were applied to the AACs. In the production of AACs, granulated blast furnace slag was employed as an aluminosilicate-rich raw material, and a sodium silicate and sodium hydroxide combination was used as an alkaline activator. Physical properties (flowability, water absorption, capillary water absorption, and dry unit weight), and 8-h strength performances (flexural and compressive) were determined. Furthermore, to monitor the influence of high temperatures on the characteristics of the AAC, the mixtures were exposed to elevated temperatures (200, 500, and 800 °C). In SEM image analysis, it was determined that spherical CSH gels were formed in the heat-cured AACs. It has been observed that the geopolymerization products decompose in AACs exposed to 800 °C. To evaluate statistically the experimental results, a multi-factor analysis of variance (ANOVA) was also applied. The results revealed that increasing the coarser fine aggregate fraction led to higher water absorption and apparent porosity capacities and lower unit weight. Besides, strength performance was improved by applying a heat-curing strategy to the AAC, whereas a decrease was observed by increasing the No.5 CA fraction. There was a remarkable reduction in compressive strength and considerable loss of mass when the AAC mixes were exposed to high temperatures.

Keywords Alkali-activated mortar · Clinker aggregate · Elevated temperature · Physical properties · Strength performance

✉ Süleyman İpek
sipek@bingol.edu.tr

Barış Bayrak
bbayrak@kafkas.edu.tr

Haluk Görkem Alcan
hgorkemalcan@kafkas.edu.tr

Gökhan Kaplan
gkaplan@atauni.edu.tr

Abdulkadir Cüneyt Aydın
acaydin@atauni.edu.tr

Erhan Güneyisi
eguneyisi@harran.edu.tr

[1] Department of Civil Engineering, Kafkas University, 36100 Kars, Turkey

[2] Department of Civil Engineering, Bingöl University, 12000 Bingöl, Turkey

[3] Department of Civil Engineering, Atatürk University, 25240 Erzurum, Turkey

[4] Department of Civil Engineering, Harran University, 63300 Şanlıurfa, Turkey

Abbreviations

AAC	Alkali-activated composite
CA	Clinker aggregate
CW	Colemanite waste
GBFS	Granulated blast furnace slag
No.10	Particle size ranging from 0 to 2 mm
No.5	Particle size ranging from 2 to 4 mm

1 Introduction

The rapidly urbanizing globe produces a significant and incremental decline in natural resources due to the fact that urbanization necessitates the use of traditional concrete as a construction material [21, 26]. Conventional concrete, which consists mostly of cement, aggregate, and water, is typically responsible for utilizing basic resources for both the production and manufacturing of cement. The manufacturing of cement, the primary binder ingredient in typical concrete, accounts for approximately 5% [25], 6% [48], 7% [22], and 8% [1] of all human-caused worldwide carbon emissions. Cement is classified as an ecologically hazardous binder material, since CO_2 is recognized as a substantial contributor to the production of greenhouse gases that contribute to climate change [25]. To enhance resource efficiency and minimize energy consumption, low-carbon, low-emission, and energy-saving green cementitious materials need to be developed. In recent years, low-carbon alkali-activated materials and green hybrid alkaline cement have been developed to replace cement and address difficulties associated with the manufacturing of cement. These materials are predicted to contribute to the reduction of CO_2 emissions. Instead of hydration interactions between water and cement, this new method handles the hardening process through polymerization reactions between the aluminosilicate raw materials and the alkaline activator. This innovative material is able to meet the raw material requirements for the polymerization process, using industrial waste materials like blast furnace slags, fly ash, bottom ashes, waste glass, etc.

This composite concept is more energy-efficient and environmentally friendly than traditional building materials, because it does not require cement as a binder, resulting in lower energy consumption (about 40%) and greenhouse gas emissions (nearly 70%) [34], thereby reducing carbon footprint of concrete manufactured with ordinary Portland cement [46]. In addition to its environmental and energy-efficient aspects, AAC possesses robust mechanical capabilities, durability, and resilience in harsh environments, making it an excellent material for civil engineering applications [28]. Using several alkaline concentrations [47], changing binder-aggregate types [26] and particle size [23], reinforcing by different types of fiber such as polyvinyl alcohol fiber [30] and basalt fiber, glass fiber, and steel fiber [34], and optimizing chemical composition with mineral additives [10] have all been studied to enhance the mechanical and durability performances of AAC. In this context, AAC is well known for its ability to withstand high temperatures [11]. According to Li et al. [32], AAC that is exposed to high temperatures may develop small cracks, but it does not spall. The literature shows that AAC experiences a significant reduction in strength performance when exposed to temperature of higher than 600 °C [29] and increase after 800 °C [41]. However, in these studies, the structure for the aggregate phase in the composites still relies on basic sources. Although some studies have incorporated different types of aggregate into AAC production, the literature on this topic remains insufficient. For example, the thermal behavior of geopolymer composites using chamotte aggregate was investigated by Rovnanik and Safrankova [42] and it was concluded that chamotte aggregate decreases mechanical performance while increasing the thermal stability of the geopolymers. Mermerdaş et al. [35] evaluated the effect of various aggregate types, such as crushed limestone and river sand, on the properties of geopolymer composites. According to this study, the geopolymer composite had better flowability when made with river sand. Additionally, it exhibited higher compressive and tensile strengths when made with crushed limestone. Mohseni et al. [36] evaluated the performance of geopolymer composite using low-density aggregate derived from scoria rock. It was shown that replacing 20% of the natural sand with scoria particles resulted in inferior durability performance. Ekmen et al. [20] investigated the fresh and hardened state characteristics of geopolymer composites including 35% pumice aggregate and concluded that there is a complex interaction between the pumice aggregate and matrix phase. Li et al. [31] inspected the mechanical characteristics of a geopolymer composite incorporating standard and river sand of varying gradations. According to Carabba et al. [17], lightweight aggregate-based AAC may exhibit superior performance than traditional cement-based counterparts. In another study, İpek [26] conducted an experimental study on the impact of fly ash pellets (as lightweight aggregate) and recycled sand from construction materials (as normal weight aggregate) on the engineering properties of geopolymer composites. The study aimed to determine the effect of these fine aggregates on the properties of the geopolymer composites. The study found that recycling basalt, granite, marble, and ceramic tiles to produce fine aggregate has little effect on the strength performance of geopolymers. However, the use of fly ash pellets and recycled concrete aggregate has a significant negative impact on strength performance. In this context, the conclusion was established that aggregate gradation has a crucial impact on the mechanical characteristics of geopolymer composites.

However, some studies in the literature have replaced natural sand with CA of varying sizes and contents. One of them was carried out by Bayrak et al. [13], in which the physicomechanical properties of high-temperature exposed AACs manufactured with CA cured under different regimes were investigated. They reported flexural and compressive strengths of more than 5 and 40 MPa, respectively, in AAC mixes including CA. In a study carried out by Berger [14], natural aggregate was replaced with PC clinker in concrete due to the reactivity of natural aggregate when it comes into contact with water, which creates binding chemicals on its surface. By employing PC clinker, the researcher was able to avoid this issue and create stronger, more durable concrete. Besides, the researcher concluded that this substitution results in concrete with a maximum aggregate size restriction of approximately 9.5 mm and significantly enhances the mechanical properties of the mixture. Shafaghat and Allahverdi [45] conducted a study investigating the effects of replacing aggregate larger than 1 mm with PC clinker of the same size on concrete characteristics. The study reported that enhancing the ITZ microstructure resulted in significant improvements in concrete characteristics.

2 Research significance

AAC has not been extensively tested for its performance under high temperatures. For this reason, it may be worth noting that further testing is required to determine the performance of AAC exposed to high temperatures (200, 500, and 800 °C). It is important to carefully analyze the mechanical and thermal properties of these materials when exposed to fire to guarantee the safety of individuals and assets during the construction process. This study examines the performance of GBFS-based AAC at elevated temperatures to showcase the advantages of these composites while acknowledging the value of other construction materials. For this purpose, four AAC mixtures based on GBFS were designed and manufactured in the current study. Furthermore, as part of this study, the impact of different curing strategies (ambient, 45, and 75 °C temperatures) on the engineering properties and high-temperature performance of AAC mixtures was assessed. The aluminosilicate-rich raw material in the mixtures was activated by a mixture of sodium silicate (Na_2SiO_3) and sodium hydroxide (NaOH). The aggregate used to produce AAC mixtures consisted of CA aggregate of various particle sizes, including medium aggregate (4–8 mm), No.5 (2–4 mm), and No.10 (0–2 mm). The study further analyzed the impact of the fine CA-size fraction on the performance of AAC mixtures, while the fraction of the medium CA was kept constant in all mixtures. This study is significant, because there is a limited amount of research on the utilization of CA in geopolymer composites and AAC in the existing literature. AAC has a greater ability to resist microstructural damage than traditional mortars and concrete when exposed to high temperatures. The network of pores inside the gel and matrix, however, limits the transport of moisture when subjected to high temperatures. Therefore, the mechanical stability of AAC is highly dependent on its microstructure. Therefore, this study also examined the microstructural characteristics of ACC mixtures. From this standpoint, the study adds many new and crucial results and findings to the literature on building and construction materials in terms of sustainability and environmentally friendly material production.

3 Experimental programs

3.1 Materials

This study used GBFS conforming to ASTM 989 [9] standard as the aluminosilicate-rich material in the production of AAC mixtures. The specific surface area (Blaine method) and specific gravity of GBFS were 4500 cm^2/g and 2.81, respectively. The mineralogical characteristic of GBFS is given in Fig. 1. In addition, waste colemanite having a maximum particle size of less than 1000 µm was used as a filling material in the mixtures. The specific gravity of waste colemanite was found to be 2.48. The chemical compositions of GBFS and waste colemanite are presented in Table 1.

For the chemical activation of GBFS, a 1 to 2.5 mixture of 12 M NaOH and Na_2SiO_3 solutions were used as alkaline activators. The Na_2SiO_3 had a modulus ratio (SiO_2/Na_2O) of 3.19 (wt% SiO_2: 28.25% and Na_2O: 8.85%) and a specific gravity of 1.38. The 12 M NaOH solution has a density of 1.38 kg/cm^3 at 20 °C and was prepared using 99%

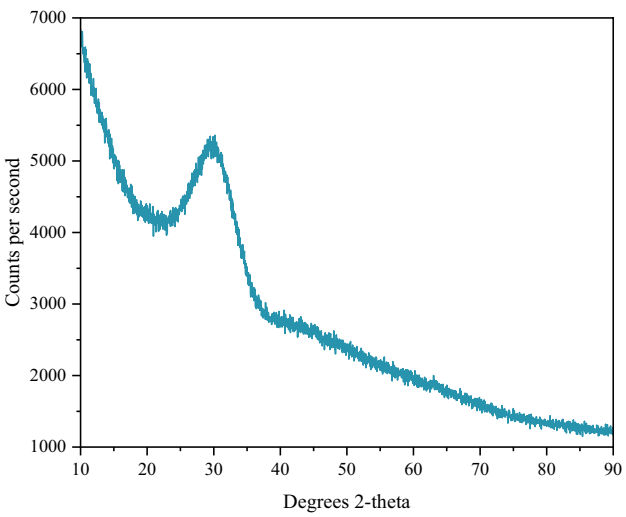


Fig. 1 XRD pattern of GGBFS

Table 1 Chemical characteristics of GBFS and waste colemanite

Materials	Compositions (%)								LOI*
	CaO	SiO_2	B_2O_5	Al_2O_3	Fe_2O_3	K_2O	MgO	SO_3	
GGBFS	43.1	32.6	<0.1	12.3	1.5	0.2	6.6	1.3	2.0
Waste colemanite	37.5	15.1	13.2	0.8	0.3	0.2	13.6	0.4	17.4

*Loss on ignition

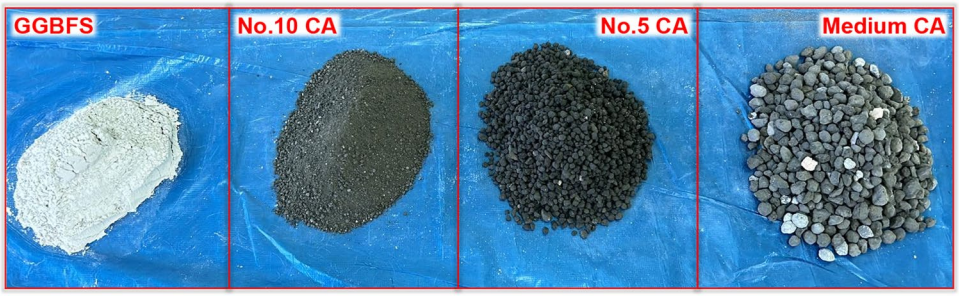


Fig. 2 Photographic views of GGBFS, No.10 CA, No.5 CA, and medium CA

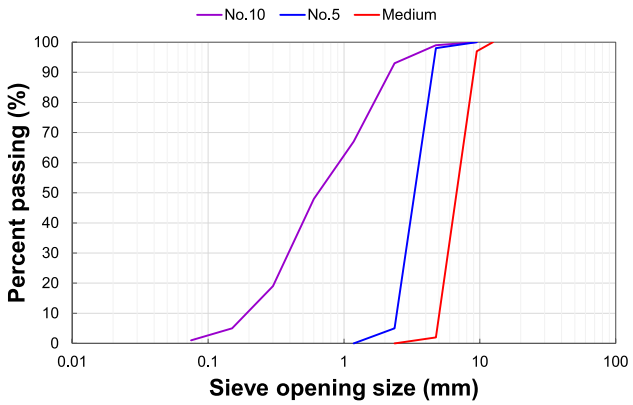


Fig. 3 Sieve analysis results of CAs

pure NaOH in a white flake form. No superplasticizer or additional water was employed for the production of AAC mixtures.

As an aggregate, cement clinker in different particle sizes was used for the production of the mixtures. CAs used for the production are classified according to particle size into three groups: No.10 having particle size varying between 0 and 2 mm, No.5 having particle size varying between 2 and 4 mm, and a medium having a particle size ranging from 4 to 8 mm. The photographic views of GBFS, No.10 CA, No.5 CA, and medium CA are presented in Fig. 2. The gradation curves of CAs are given in Fig. 3 and their physical properties are listed in Table 2.

3.2 Mix proportions and production process

The mix proportions in Table 3 were used for the preparation of the AAC samples. In the preparation of all mixtures, the amount of GBFS and waste colemanite was kept constant at 600 and 100 kg/m^3, respectively. The GBFS-to-alkaline solution (sodium silicate + sodium hydroxide) ratio was designated as 1.2-to-1. The amount of the alkaline solution was determined according to sufficient workability. The alkali solution's sodium silicate-to-sodium hydroxide ratio was set at 2.5. Three different curing strategies—ambient, 45, and 75 °C temperatures—were applied to the AAC mixtures for 8 h.

The 12 M sodium hydroxide solution was prepared 24 h prior to casting. The mixtures were manufactured using

Table 2 Physical properties of CAs

Properties	No.10	No.5	Medium
Particle size (mm)	0–2	2–4	4–8
Specific gravity	2.91	2.86	2.84
24-h water absorption (%)	0.8	0.6	0.5
Fineness modulus	2.88	3.98	5.78
Color	Dark gray	Dark gray	Dark gray

Table 3 Ingredient weights used in the production of AAC composites (in kg/m^3)

Ingredients		Mix1	Mix2	Mix3	Mix4
GBFS		600	600	600	600
Colemanite		100	100	100	100
Fine aggregate	Clinker (No.10)	800	700	600	500
	Clinker (No.5)	200	300	400	500
Medium aggregate	Clinker (4–8)	100	100	100	100
NaOH		143	143	143	143
Na_2SiO_3		357	357	357	357

a Hobart mixer of the laboratory variety. The first step involved mixing GBFS and waste colemanite for 1 min at 145 rpm. The mixture was then mixed at 145 rpm for 1 min and 280 rpm for 2 min, while the alkali solutions (sodium hydroxide and sodium silicate) were added. After adding the clinker aggregates, the mixture was then mixed at 145 rpm for 1 min and 280 rpm for 3 min. The flow table test was first performed on the fresh AAC mixtures, and each mix was then placed in the molds. The molded mixes were placed into the oven immediately after being placed into a nylon bag during the heat-curing process, whereas new mixes were just placed inside a nylon bag and remained at ambient temperature during the curing procedure. A laboratory-type oven with a temperature increase of 5 °C/min was employed in the heat-curing strategies. After reaching the required temperature (45–75 °C), the specimens were maintained in the oven for 8 h in a sealed bag with 70% relative humidity condition. Following an 8-h heat-curing time, the samples were cooled in the oven until they reached laboratory temperature before being tested.

3.3 Methods

The flow table test was performed per ASTM C1437 [5]. The unit weight of AAC mixes was determined following the ASTM C138 [4], while the water absorption capacity and apparent porosity of the mixtures were measured in regard to the ASTM C642 [8]. The interconnected pores play a significant role in the durability performance of such composites. Therefore, it is very important to determine the amount of interconnected pores. The sorptivity test is a simple and quick method for indirectly measuring the amount of these pores, which is used to determine the water absorption tendency through capillary suction formed in the interconnected pores of such composites. Here, BS EN1015-18 [16] was followed to measure the capillary water absorption capacity of the AAC samples. Unit weight, water absorption capacity, and apparent porosity of the mixtures were determined after 8 h of the curing period, while capillary water absorption values were established after 24 h. The mechanical performance of the ACC mixtures was determined based on flexural and compressive strength tests, which were, respectively, conducted according to ASTM C349 [7] and ASTM C348 [6]. The samples with the dimensions of 40 mm by 40 mm by 160 mm were used to observe the strength characteristics of mixes. Three samples of each AAC mixture were taken for each test, and their averages with error bars are presented as the final results.

Withal, the mass loss and compressive strength of AAC mixes cured using different curing procedures were examined after exposure to temperatures of 200, 500, and 800 °C to investigate the high-temperature effect. For this purpose, a muffle furnace with a heating rate of 10 °C/min was employed. Once the oven temperature had reached the target temperature (stage 1), the samples were left in the oven for 1 h (stage 2). This process of high-temperature application is graphically indicated in Fig. 4. The samples were cooled in the furnace until they reached laboratory temperature (Stage 3), and then, the mass loss and compressive strength of the mixes were determined.

4 Results and discussion

4.1 Physical properties

4.1.1 Flowability

The flowability characteristic of the AAC mixes, examined per the flow table test, indicated that all mixtures had more than 100% flowability, which means perfect spreading, as visualized in Fig. 5. Furthermore, it would be seen that increasing the No.5 (coarser) CA fraction in the ACC leads to a marked increase in the flowability of the mixes. Increasing the No.5 CA fraction from 20 to 50% increased the flowability of AAC mixtures from 202 mm (102%) to 221 mm (121%). This increased flow diameter by approximately 10%. The most significant factor leading to this increment is the difference between the fineness moduli of No.10 and No.5 CAs, which empirically represents the difference between the mean size of their particles. In addition, it is well known that an indirect idea about the specific surface area of the aggregate can be evaluated by looking at its fineness modulus. In the literature, it has been reported

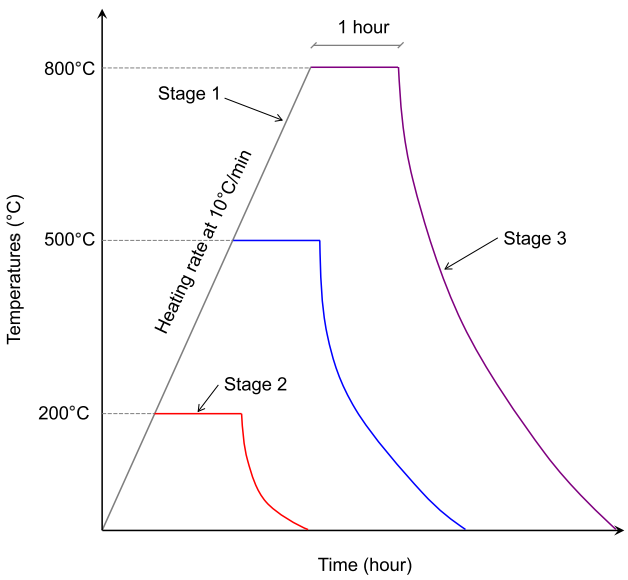


Fig. 4 Graphical demonstration of the high-temperature application process

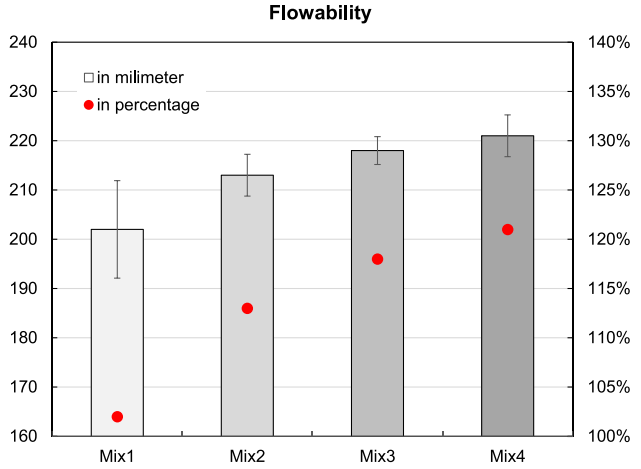


Fig. 5 The variation in flowability of AAC mixtures

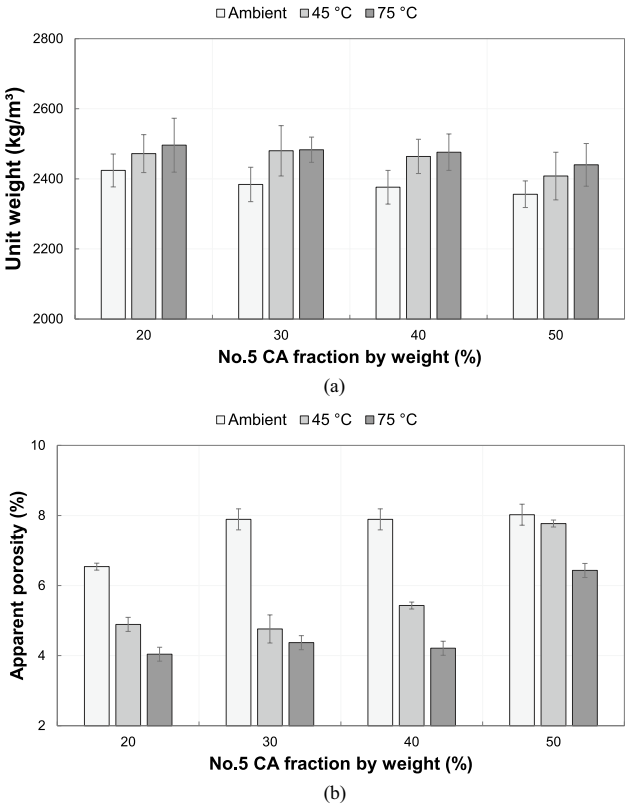


Fig. 6 The effects of curing strategy and No.5 CA fraction on **a** the unit weight and **b** the apparent porosity of AAC mixtures

that there is an inverse relationship between the fineness modulus of the aggregate and its specific surface area; in other words, the higher the fineness modulus, the lower the specific surface area. In this regard, the specific surface area would be used as a tool to get an idea about the amount of water needed to get the aggregate wet. The fineness modulus of the No.5 CA is about 4.0, while that of the No.10 type is nearly 2.9, as presented in Table 2. This would numerically indicate that the No.5 CA has a lower specific surface area than the No.10 type. As a consequence of this, replacing the No.10 CA with the No.5 type has resulted in less mixing water being consumed to wet the aggregate, leading to higher flowability. Another factor leading to the higher flowability due to the increasing No.5 fraction is the relatively lower water absorption capacity of No.5 CA. Again, when the physical properties of CAs listed in Table 2 are investigated, it is seen that the No.10 CA with particle size varying between 2 and 4 mm has a 24-h water absorption capacity of 0.6%, while the No.5 type aggregate with particle size ranging from 0 to 2 mm has that of 0.8%. Soever, the difference between the 24-h water absorption capacities of these two different sizes of fine aggregate is small, and it may have played a role in increasing the mixture's flowability.

4.1.2 Unit weight and apparent porosity

Substitution of No.10 CA with No.5 type also has influenced both the unit weight and the apparent porosity values of ACC mixtures. The changes in apparent porosity and unit weight of the AAC mixtures cured at various strategies with respect to the No.5 clinker aggregate fraction are visualized in Fig. 6a, b, respectively. The unit weights of AAC mixtures produced with a fine aggregate mix of 80% No.10 and 20% No.5 CAs and cured at ambient, 45, and 75 °C temperatures were 2424, 2472, and 2496 kg/m^3, respectively. As can be understood from Fig. 6a, gradually increasing the No.5 CA fraction from 20 to 50% resulted in systematic decreases in the unit weights of AAC samples at all curing strategies. The overall reduction in unit weights of AAC mixes was between 2 and 3% for all curing strategies. The main reason for this scenario is of course the relatively lower specific gravity of No.5 CA. As is well known, replacing something heavy with something lightweight in such a system would cause a decrease in unit weight. Withal, increments in the unit weight varying between 2 and 4% and between 3 and 4.2% were observed when the 45 and 75 °C curing strategies were applied to the AAC mixtures, respectively. However, when both the small amount of variations in unit weight depending on No.5 CA fraction and curing strategy and especially the error bars given in Fig. 6a are considered, it can be stated that the unit weights of AAC mixes are close to each other; so, the difference can be neglected. The unit weight ranged from 2350 to 2500 kg/m^3 in the AAC mixtures manufactured in this study. The apparent porosity of the Mix1 AAC mixture, which included a fine aggregate mixture consisting of 80% No.10 and 20% No.5 CAs, has been measured at nearly 6.5% when it was cured at ambient temperature. However, as can be seen in Fig. 6b, applying heat curing to

the mixtures led to decreasing the apparent porosity to 4.9% and 4.0% when Mix1 was cured at the 45 °C and 75 °C curing regimes, respectively. It can be stated as a consequence that a lower porosity in the mixtures may have been achieved by the heat curing since the geopolimerization reaction may have taken place at a greater rate as the temperature rises. At the initial phase, the pores in the medium are slightly large; however, they are gradually filled with gels that continue to grow as they are cured, and the progress of geopolymerization makes way for the formation of longer chains and branches. With rising curing temperatures, especially in the early stage of the geopolymerization process, the degree of precursor dissolution from the amorphous phases in the aluminosilicate-rich raw material particles increases, and the formation of hard structures accelerates [15]. As a result of using the elevated temperature curing regime at an early stage, the amount of pores in the AAC is reduced. The results, on the other hand, indicated that increasing the No.5 CA fraction caused the AAC mixtures to have higher porosity values. The apparent porosity of the ACC mixture cured at ambient temperature increased from 6.5% to about 8.0% when the fraction of No.5 CA in the fine aggregate was increased from 20% to 50%. A similar trend of increase in the apparent porosity depending on the No.5 CA fraction was also observed in the AAC mixtures cured at 45 °C and 75 °C. As shown in Fig. 6b, it was increased from 4.9% to about 7.8% in the case of the application of a 45 °C curing strategy and from about 4% to 6.4% in the case of a 75 °C curing strategy. The main reason causing this increment is directly related to the gradation of fine aggregate. The quantity of gaps (or pores) that are required to be filled tends to increase as the aggregate coarsens [2, 3]. According to Basheer et al. [12], one of the main reasons for this is the increase in local porosity in the interfacial transition zone. In addition, the tendency for bleeding water to be collected under the coarse aggregate particles may also be a reason why the amount of gaps (pores) in the concrete structure increases with the coarsening of the aggregate [12]. Therefore, the substitution of No.10 CA having particles between 0 and 2 mm with No.5 CA having particles between 2 and 4 mm will result in an increase in both the amount and distribution of gaps (or pores) in the AAC structure.

4.1.3 Water absorption and capillary water absorption

The effects of the curing regime and the No.5 CA fraction on the water absorption and capillary water absorption of AAC mixes are, respectively, indicated in Fig. 7a, b. The results showed that the average water absorption and capillary water absorption capacities of Mix1 cured at the ambient temperature were about 8.4% and 0.88 kg/m^2, respectively. Increasing the No.5 CA fraction has generally tended to increase both absorption capacities regardless of curing

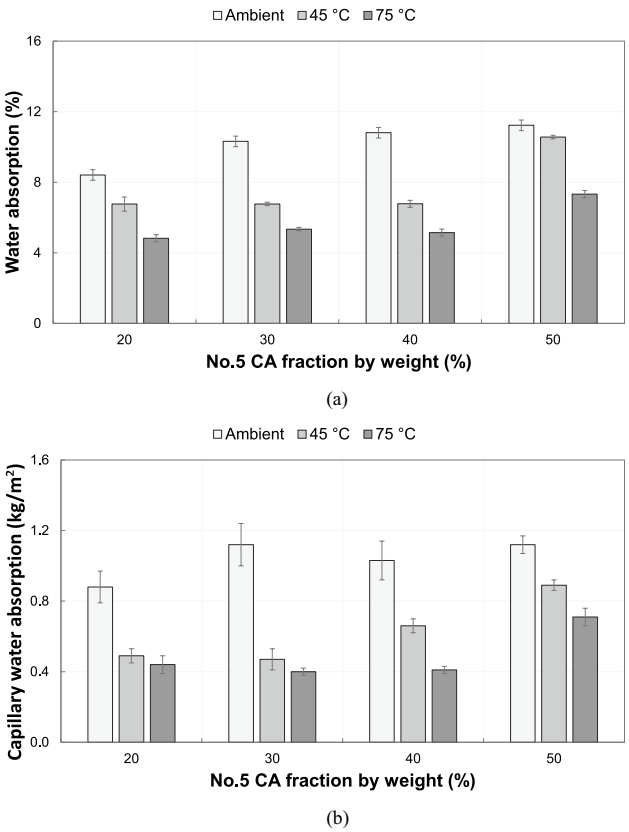


Fig. 7 The effects of curing strategy and No.5 CA fraction on **a** the water absorption and **b** capillary water absorption of AAC mixtures

strategy type. Even though there were slight fluctuations in both water absorption capacities due to the gradual increase of the No.5 CA fraction from 20 to 50%, the final effect of increasing the No.5 CA fraction was an increasing effect, as can be seen in Fig. 7a, b. Applying heat curing to the AAC mixtures, on the other hand, improved their water absorption performances. The average water absorption capacity of Mix1 cured at the 45 and 75 °C temperatures were, respectively, about 6.8 and 4.8%, whereas its average capillary water absorption capacities were 0.49 and 0.44 kg/m^2 when it was cured at the same temperatures, respectively. Approximately 34, 56, and 52% increments were observed in the water absorption capacities of the AAC mixes cured, respectively, at ambient, 45, and 75 °C temperatures when the No.5 CA fraction was increased from 20 to 50%. The increments in the average capillary water absorption capacities of the AAC mixes cured at ambient, 45 °C, and 75 °C temperatures due to increasing the No.5 CA fraction were, respectively, about 27, 82, and 61%. The decreases in the water absorption capacities in Mix1 due to the application of 45 and 75 °C heat curing were nearly 20 and 43%, respectively, while those in the capillary water absorption capacities were about 44 and 50%, respectively.

A similar observation regarding the effect of heat curing on the water absorption performance of AACs was reported by Noushini and Castel [38]. They have investigated the water absorption capacity and sorptivity performances of alkali-activated fly ash composites cured at various temperatures and found an enhancement in water absorption performance as the curing temperature rises. They attributed this result to the high degree of geopolymerization due to the elevated curing temperature and the consequent formation of dense molecular structure. Another important study in this regard was carried out by Kaplan et al. [27]. The influences of curing temperature on some early age features of high-strength alkali-activated GBFS composites were investigated. A more than 6% decrease in the capillary water absorption capacity of the AACs has been reported when they increased the curing temperature from 40 to 60 °C. They ascribed this reduction to the decrease in capillary void size as a result of heat curing and the formation of a denser gel structure.

4.1.4 The relationship between physical properties

To observe whether a bilateral relationship exists between the investigated physical properties of AAC blends, the bilateral correlations between these properties were examined in this section. The relationships between apparent porosity and unit weight, water absorption and unit weight, apparent porosity and water absorption, and capillary water absorption and water absorption are shown in Fig. 8a–d, respectively. A strong linear relationship was established between all investigated physical properties of the AAC samples with an R-square value higher than 0.9. Besides, it was seen that there was an inverse correlation between the apparent porosity and unit weight of the AAC samples; namely, as the unit weight increased, the apparent porosity decreased. An identical correlation was also observed between the water absorption and unit weight of the AAC mixtures. On the other hand, it was seen that there were direct correlations between apparent porosity and water absorption and between capillary water absorption and water absorption capacities of the AAC mixes. These findings are an indication that both the results of this study were not achieved by chance, and a systematic experimental program was conducted within this work.

4.2 Strength characteristics

One of the important aspects of the current study is the investigation of the early age strength performance of AAC mixtures manufactured in different fine aggregate-size fractions and cured under various curing strategies. For this purpose, the 8-h average flexural strengths of the mixtures were first determined, and the compressive strengths were then inspected using portions of prisms broken in flexure. In this context, the 8-h average flexural and compressive strengths of ACC mixtures are visualized in Fig. 9a, b, respectively. The ambient temperature-cured Mix1 that was manufactured with a fine aggregate mixture consisting of 80% of No.10 and 20% of No.5 CAs had an 8-h average flexural strength of nearly 3.9 MPa, and a systematic decrease in the flexural strength was observed as the No.5 CA fraction was gradually increased from 20 to 50%. The 8-h average flexural strength of ambient temperature-cured Mix4 that was manufactured with a fine aggregate mixture consisting of 50% of No.10 and 50% of No.5 CAs was about 3.0 MPa. Withal, the application of heat curing and increasing the applied temperature of curing increased the 8-h flexural strengths. The 8-h average flexural strengths of the 45 °C heat-cured AAC mixtures were between roughly 3.7 and 4.5 MPa, while those of the 75 °C heat-cured AAC mixtures were between about 4.7 and 5.4 MPa. The 8-h average flexural strengths of the Mix1 named mixture were, respectively, about 4.5 and 5.4 MPa when 45 and 75 °C heat curing strategies were applied. An increase of more than 10% in the flexural strength of the AAC mixtures was obtained by applying a curing temperature of 45 °C, while an increase of more than 35% was obtained by applying a curing temperature of 75 °C. However, increasing the No.5 CA fraction caused a decrease in the 8-h flexural strength of the AAC mixtures cured at the ambient temperature of 24%, whereas about 19 and 11% decreases were determined in the ACC mixes cured at 45 and 75 °C curing temperatures, respectively.

As can be seen in Fig. 9b, a similar trend was determined in the 8-h average compressive strength of AAC mixtures. Increasing the No.5 CA fraction yielded a lower compressive strength of ACC mixtures while applying heat curing and increasing the heating temperature led to an enhancement in the compressive strength. The Mix1 labeled mixture cured at the ambient temperature had an 8-h average compressive strength of nearly 40 MPa, and gradually increasing the No.5 CA fraction from 20 to 50% caused a systematic decrease in the compressive strength to nearly 25 MPa. The same mixture exhibited approximately 54 MPa and 66 MPa 8-hcompressive strength performances when 45 and 75 °C heat-curing strategies were applied. The use of a 45 °C heat-curing regime raised the 8-h compressive strength of AAC mixes by 30–65%, whereas using a 75 °C heat-curing regime increased it by 65 to 125%. The 8- average compressive strengths of the 45 °C heat-cured AAC mixtures were between roughly 35 and 54 MPa, whereas those of the 75 °C heat-cured AAC mixtures were between 55 and 66 MPa. Increasing the No.5 CA fraction also decreased the compressive strength of the heat-cured AAC mixtures; however, the amount of reduction due to the No.5 CA fraction was not as great as in the ambient temperature-cured mixtures.

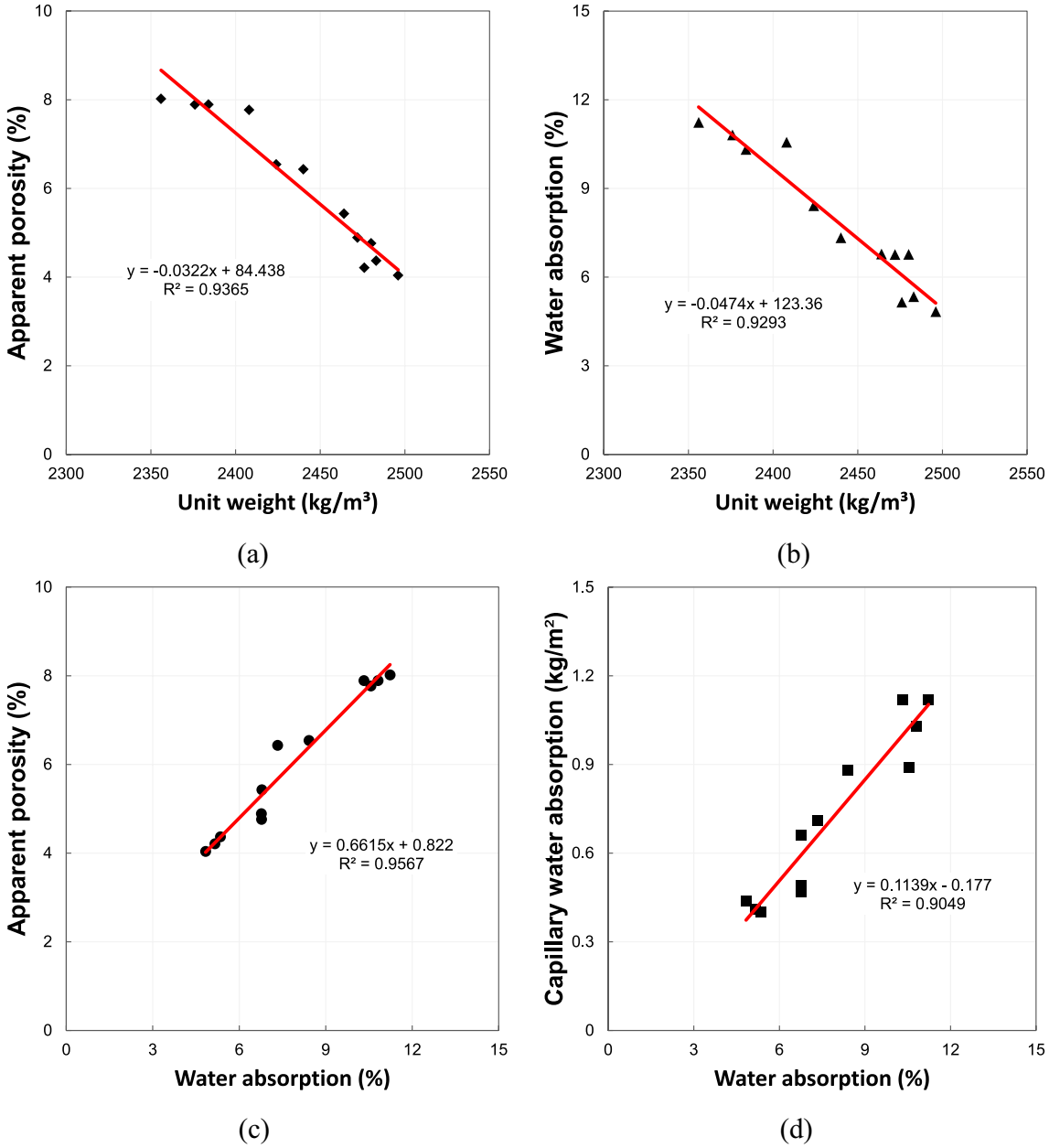
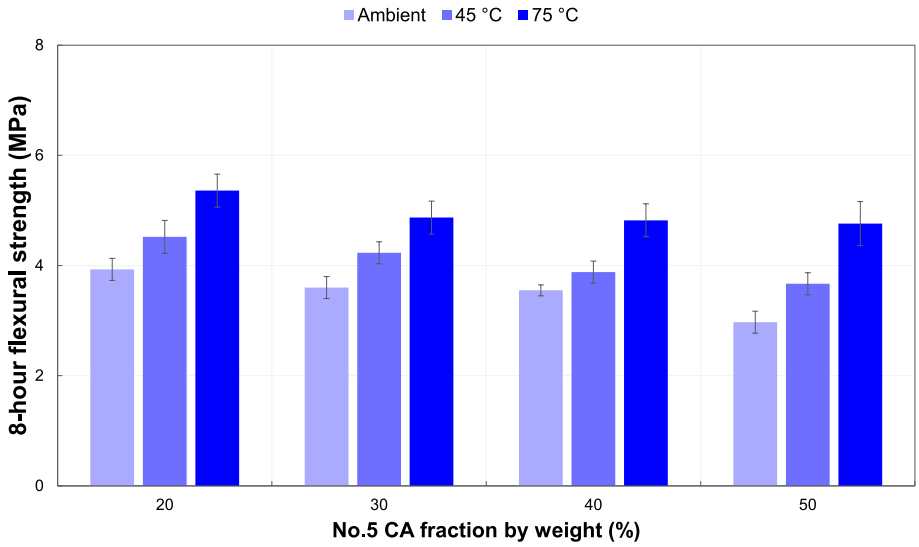
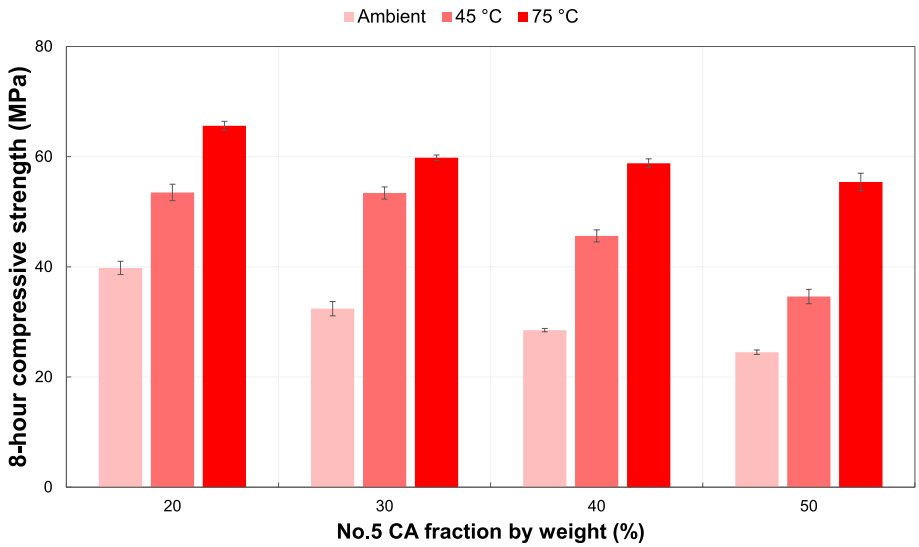


Fig. 8 The relationship between **a** apparent porosity and unit weight, **b** water absorption and unit weight, **c** apparent porosity and water absorption, and **d** capillary water absorption and water absorption

The enhancement in the strength performance of such composites with increasing curing temperatures can be regarded as a general phenomenon. There is a strong relationship between geopolymerization and the early age heat curing temperature and time. The geopolymerization at an early age and indirectly its amount of products significantly depend on the curing temperature level. As a result of a high degree of geopolymerization and thus a high amount of geopolymerization products, early strength development increases with increasing curing temperature [43]. This is due to the mobility of highly activated Na^+ and OH^- ions at higher curing temperatures, which results in the formation of highly dense sodium-aluminosilicate crystals [44]. Moreover, higher temperatures result in a faster rate of strength growth because the polymerization reaction has a greater ability to change 2D polymer chains into 3D polymer chains with a stronger bond [24, 37]. Additionally, Rovnanik revealed by conducting an infrared spectrometric analysis that rising the applied curing temperature reduces the amount of unreacted solid particles in the aluminosilicate source material [43]. They did, however, observe a steady rise in the strength performance of alkali-activated



(a)



(b)

Fig. 9 The variation in 8-h **a** flexural and **b** compressive strengths of AAC mixtures in regard to curing strategy and No.5 CA fraction

fly ash composites when the curing temperature was steadily elevated from 20 to 60 °C. A similar improvement in the strength characteristics of AACs due to increasing the heating temperature from 25 to 80 °C was reported by Zhang et al. who also investigated the effect of curing temperature on the properties of alkali-activated fly ash composites [49]. Additionally, Noushini and Castel also reported a significant increase in the compressive strength of AACs when both the heat curing temperature and its application time in the early period is increased [38]. Li and Liu who examined the influence of heat-curing temperature and slag incorporation on the characteristics of AACs found a more than 30% increase in the compressive strength of alkali-activated fly ash/slag composites when they raised the heat-curing temperature from 30 to 70 °C [33]. Albeit, there is a prevalent opinion in the literature that increasing the curing temperature does not continually improve strength performance [40, 44]. Especially, continuing the application of heat curing after early periods results in a decrease in the strength performance of AACs. For example, Rovnanik observed an enhancement in both flexural and compressive strengths until 40 °C heat curing, whereas there was a slight decrease after this heat curing temperature level [43]. Also, Chithambaram et al. showed a reduction in compressive strength as curing temperature was raised above 90 °C [18]. Similarly, relatively lower compressive strengths in AACs were observed after 60 °C by Sajan et al. [44]. The causes of this scenario include the formation of additional microcracks and the loss of excessive moisture at a further increase in curing temperature.

In another respect, when the strength characteristics of AACs manufactured in this study are analyzed on the basis of the aggregate size effect, it may be stated that increasing

aggregate size decreases strength performance, since larger aggregate size utilization results in wider aggregate–paste interfaces. The failure of such wider aggregate–paste interfaces, therefore, causes a collapse of a big region in the composite, and hence, the composite exhibits lower strength performance. Besides, the utilization of coarser aggregate particles may block the upward movement of water tending to bleed, and may cause trapping of water under aggregate particles. This might be the second significant factor for the decline in AAC strength performance owing to coarser aggregate consumption. However, it should be also known that the aggregate size is not the only aggregate characteristic directly decreasing or increasing the compressive strength. There are other significant concrete aggregate characteristics, such as surface texture, shape, aggregate strength, gradation, aggregate fraction, etc. influencing the performance of the whole composite structure. The aggregate gradation and strength may be another factor that caused a decrease in both 8-h compressive and flexural strengths.

Although there is a significant difference between the inherent behavior of cement-based composites against compressive and tensile loads, it is well known that a highly correlated mathematical relationship is established between compressive and tensile strengths. The common wisdom of this relationship is that the tensile strength of cement-based composites is about 10–15% of compressive strength [39]. However, the amount of this correlation may vary depending on the size and volume of aggregate (especially coarse aggregate), mixture proportions, binder type, and concrete type [19]. In the current study, the results revealed that there is a strong correlation with an R^2 value of nearly 0.94 between the 8-h flexural and compressive strengths of AACs, as indicated in Fig. 10. Besides, the flexural strength values determined for AAC mixtures were about 8–12% of their compressive strength. These findings are an indication that the relationship between the 8-h compressive and flexural strengths of AAC samples produced in this study is matching with the common wisdom available in the literature. In addition, it can be said according to the results of this work that stating the flexural strength of AAC is about 10% of its compressive strength would not be a misleading statement.

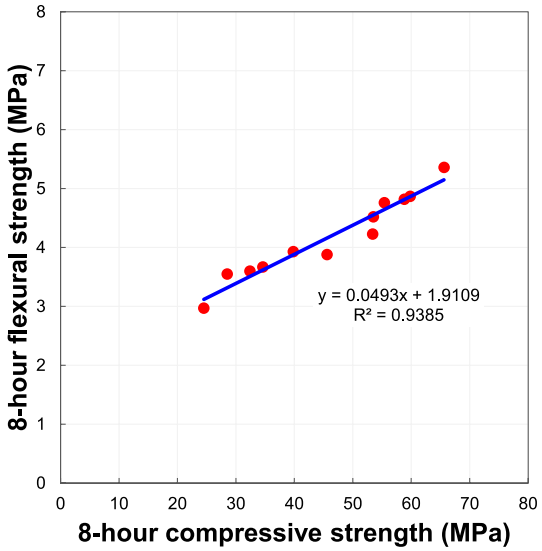


Fig. 10 The relationship between 8-h flexural and compressive strengths

4.3 Effect of elevated temperature

The original compressive strength and the percentage of residual one of the AAC mixtures exposed to elevated temperatures are given in Table 4. As can be comprehended from the table, the percent residual compressive strength values of the Mix1 labeled mixture were below 50% at 200 °C, while they were less than 35 and 20% at 500 and 800 °C, respectively. However, increasing the No.5 CA fraction resulted in higher residual compressive strength values at all high-temperature levels. Besides, it was revealed that the heat-cured AAC mixtures exhibited better performance against the elevated-temperature exposure.

The variation in compressive strength of the ambient temperature-cured AAC mixtures exposed to temperatures of 200, 500, and 800 °C is visualized in Fig. 11a. The original compressive strengths of Mix1, Mix2, Mix3, and Mix4, which were, respectively, manufactured with the No.5 CA fractions of 20, 30, 40, and 50%, were 39.8, 32.4, 28.5, and 24.5 MPa, respectively. The application of elevated temperature to the AAC mixtures caused significant reductions in their compressive strengths. The percent residual compressive strength values were below 50% when the mixtures were exposed to 200 °C, while they were less than 35 and 20% in the cases of 500 and 800 °C exposures, respectively. As the exposed temperature steadily increased from 200 to 800 °C, a systematic reduction in compressive strength was found. As presented in Fig. 11a, the average compressive strengths of Mix1, Mix2, Mix3, and Mix4 after exposure to 200 °C temperature were about 17.0, 27.8, 28.1, and 30.4 MPa, respectively, and they were reduced to 7.1, 10.4, 12.6, and 12.0 MPa, respectively, after exposure of 800 °C temperature. As seen in Fig. 11a and understood from the aforementioned strength values, increasing the No.5 CA fraction resulted in higher compressive strength at all high-temperature exposure levels. However, upon investigation of Table 4, it was observed that Mix4, which was cured at ambient temperature, exhibited better compressive strength performance after being exposed to an elevated temperature of 200 °C. This may be due to the fact that an 8-h curing period is insufficient for proper hydration formation at ambient temperature. The mass-loss values due to elevated-temperature

Table 4 8-h compressive strength and residual compressive strength in percentage after heat exposure

Mixture identification		8-h compressive strength (MPa)	Residual compressive strength (%)		
			at 200 °C	at 500 °C	at 800 °C
Mix1	Ambient temp. cured	39.8 ± 1.2	42.7	34.7	17.9
	Cured at 45 °C temp	53.5 ± 1.5	35.9	29.9	14.8
	Cured at 75 °C temp	65.6 ± 0.8	49.7	25.7	15.1
Mix2	Ambient temp. cured	32.4 ± 1.3	85.8	48.9	32.1
	Cured at 45 °C temp	53.4 ± 1.1	62.1	37.6	22.9
	Cured at 75 °C temp	59.8 ± 0.5	59.3	31.7	21.5
Mix3	Ambient temp. cured	28.5 ± 0.3	98.6	57.0	44.3
	Cured at 45 °C temp	45.6 ± 1.1	96.4	44.9	32.6
	Cured at 75 °C temp	58.8 ± 0.8	85.2	38.8	27.9
Mix4	Ambient temp. cured	24.5 ± 0.4	124.2	68.5	49.1
	Cured at 45 °C temp	34.6 ± 1.3	96.0	52.9	39.8
	Cured at 75 °C temp	55.4 ± 1.6	69.5	36.7	25.8

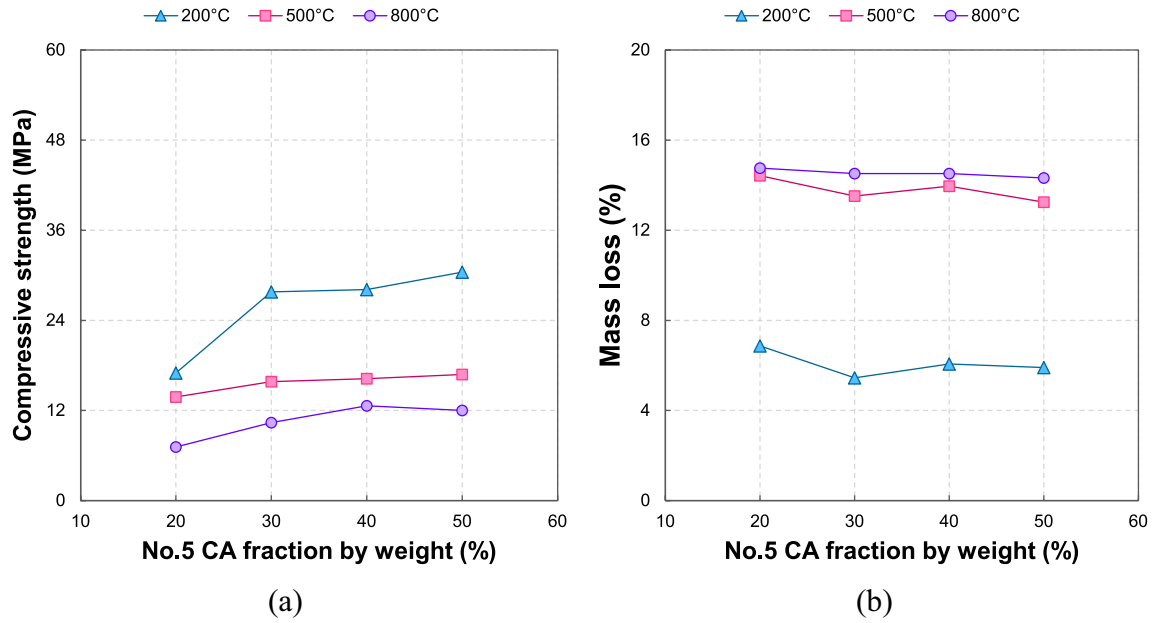


Fig. 11 The variation in **a** compressive strength and **b** mass loss of ambient-cured AAC mixtures exposed to elevated temperatures

exposure in the ambient temperature-cured ACC mixtures are indicated in Fig. 11b. The results implied that when the mixtures were exposed to a temperature of 200 °C, mass losses varying between 5 and 7% were observed. However, a much greater loss of mass was seen when the mixtures were exposed to a higher temperature. The mass-loss values of the mixtures labeled Mix1, Mix2, Mix3, and Mix4 were close to each other and ranged between 14 and 15%. It is an indication that the fraction of No.5 CA does not have a significant influence on mass loss, especially at higher temperature exposure levels.

The compressive strength and mass loss after elevated-temperature exposure of 45 °C-cured AAC mixtures are shown in Fig. 12a, b respectively. The original compressive strengths of Mix1, Mix2, Mix3, and Mix4 labeled mixtures were 53.5, 53.4, 45.6, and 34.6 MPa, respectively. They reduced to 19.2, 33.2, 44.0, and 33.2 MPa, respectively, when they were exposed to 200 °C. Dramatic decreases in compressive strength were observed when the exposure temperature was raised from 200 to 800 °C. The compressive strength values after the exposure to 800 °C of Mix1, Mix2, Mix3, and Mix4 named mixtures were 32.6, 35.5, 50.1, and 38.5 MPa, respectively. The positive effect of increasing the fraction No.5 CA was also seen in the 45 °C-cured AAC mixes when they were exposed to elevated temperatures. Steady increases were seen in the residual compressive

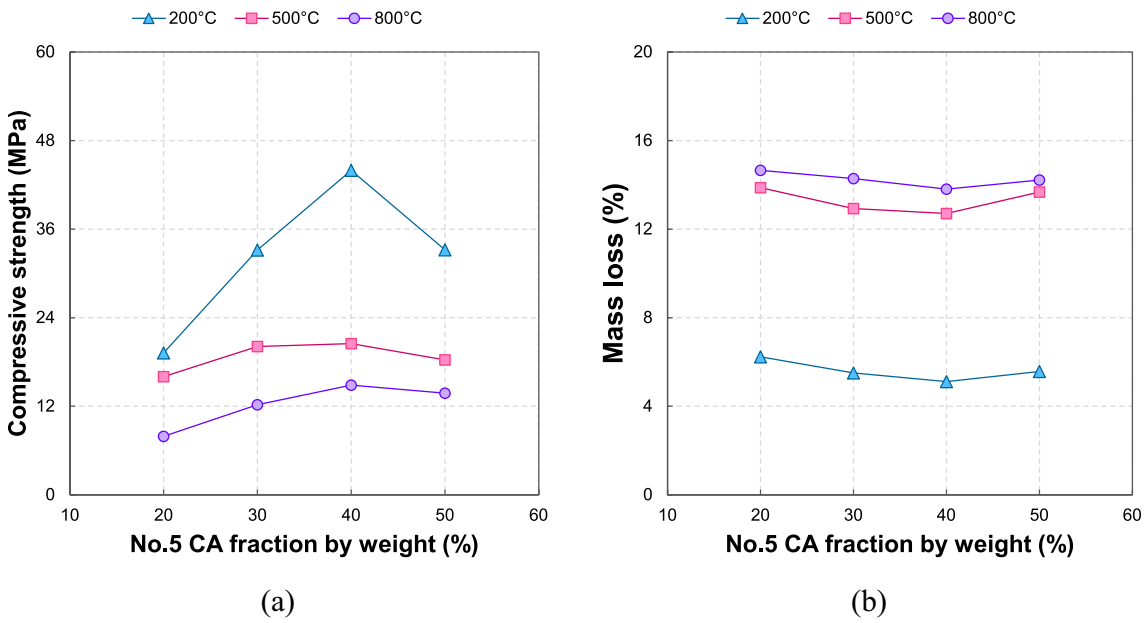


Fig. 12 The variation in **a** compressive strength and **b** mass loss of 45 °C-cured AAC mixtures exposed to elevated temperatures

strength values when the No.5 CA fraction was partially increased from 20 to 40%; however, a slight decrease was seen at the 50% fraction level. In another saying, the results of the mass loss of 45 °C-cured AAC mixes exposed to elevated temperatures revealed that the influence of curing strategies is at a negligible level. As in the ambient-cured mixtures, the 45 °C-cured AAC mixtures had also mass loss values varying between 5 and 7% when they were exposed to 200 °C. Similarly, the mass-loss values were much greater when the mixtures were exposed to a higher temperature. The mass-loss values of the 45 °C-cured mixtures were also close to each other as in the ambient-cured mixtures and were between 12 and 15%. In addition, it is not possible to say that there is an obvious and systematic effect of the No.5 CA fraction on mass loss.

Here, Fig. 13a, b indicates, respectively, the variations in compressive strength and mass loss of 75 °C-cured AAC mixtures after high-temperature exposure. When the

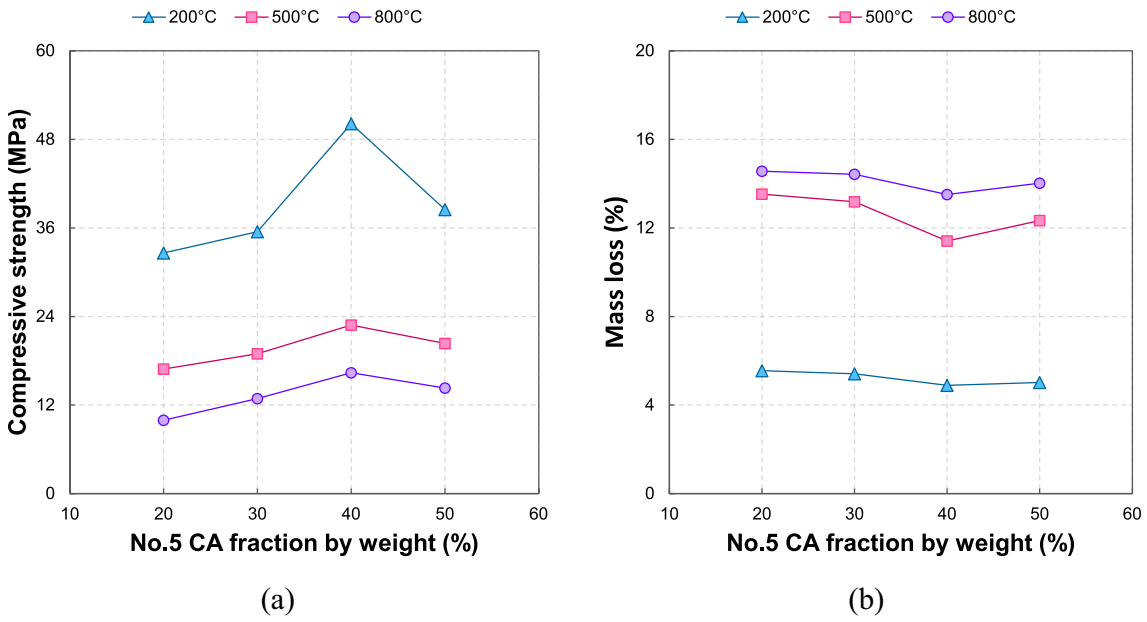


Fig. 13 The variation in **a** compressive strength and **b** mass loss of 75 °C-cured AAC mixtures exposed to elevated temperatures

results of 75 °C-cured AAC mixtures are examined, it can be understood that the 75 °C-cured AAC mixtures exhibit much better compressive strength performance compared to ambient and 45 °C-cured ACC mixtures after exposure to 200 °C. However, when exposed to temperatures of 500 and 800 °C, the compressive strength performance of the mixtures was not notably different from the ambient and 45 °C-cured mixtures. The original compressive strengths of 75 °C-cured Mix1, Mix2, Mix3, and Mix4 were 65.6, 59.8, 58.8, and 55.4 MPa, respectively. However, when exposed to 200 °C, they decreased to approximately 32.6, 35.5, 50.1, and 38.5 MPa, respectively. Their compressive strength values reduced to 16–23 MPa and 9–17 MPa when, respectively, exposed to temperatures of 500 and 800 °C. Additionally, a similar effect of the No.5 CA fraction on the residual compressive strength as in the 45 °C curing strategy was observed in the 75 °C curing strategy. Increasing the fraction of No.5 CA from 20 to 40% led to an increase in the residual compressive strength, while there was a slight decrease after this level. Typically, the 75 °C-cured ACC mixtures also exhibited similar mass-loss values to the ambient and 45 °C-cured mixtures. In another saying, there was no remarkable difference between the mass-loss values of the mixtures cured at ambient, 45, and 75 °C temperatures. For this reason, it can be stated that the curing strategies considered in this study did not exert an influence on the mass loss of the AAC mixtures exposed to high temperatures.

The bilateral relationship between mass loss and compressive strength of the AAC mixtures exposed to elevated temperature is shown in Fig. 14. When the results of all mixes subjected to 200, 500, and 800 °C were analyzed, the results indicated that there is no relevant relationship between compressive strength and mass-loss values. However, it was observed that there was a moderate relationship between the mass loss and compressive strength results of the AAC mixtures exposed to 200 °C with an R^2 value of nearly 0.83. The compressive strength and mass-loss values of AAC mixes subjected to 500 and 800 °C, besides, showed a similar association. In this regard, 200 °C may be regarded as a threshold point for the behavioral change of the AAC mixtures. In other words, as can be understood from Fig. 14, the mass loss and compressive strength results of the AAC mixtures exposed to 200 °C are clustered in a certain region, while those of the mixtures exposed to 500 and 800 °C were cumulated in a specific region.

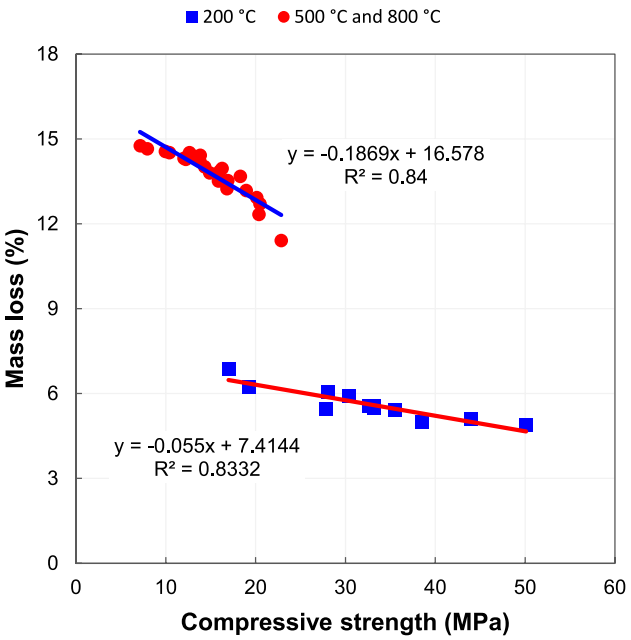
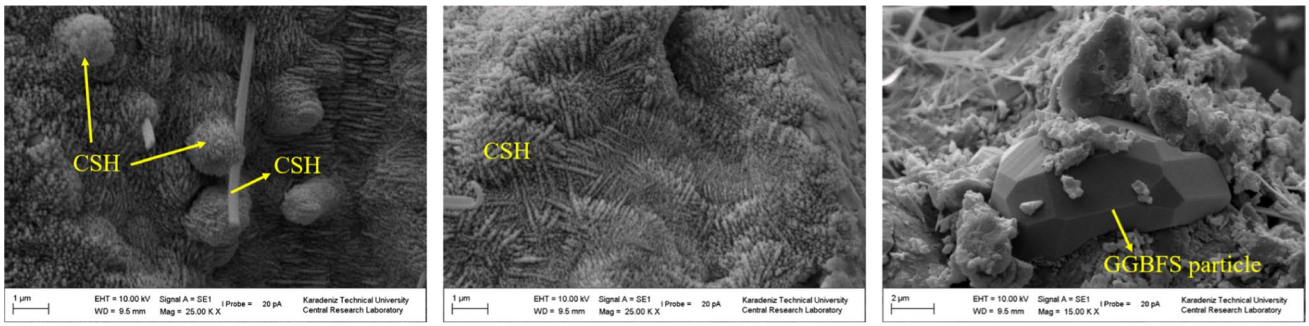


Fig. 14 The relationship between mass loss and compressive strength values after elevated-temperature exposure. **a** Mix 1 (Cured at 75 °C). **b** Mix 4 (Cured at ambient temperature)

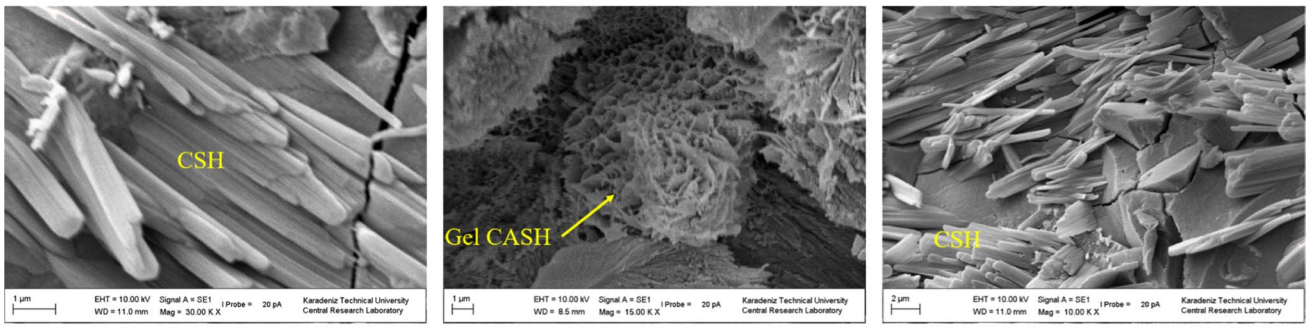
4.4 Microstructural features: SEM images

SEM images of the Mix1 mixture cured at 75 °C at different magnifications are given in Fig. 15a. It was noticed that a very dense CSH gel was formed within the matrix. The CSH gels were observed to be spherical due to accelerated geopolymerization through heat curing. The Mix1 mixture achieved the greatest compressive strength with approximately 65 MPa after 8 h. Spherical CSH gels formed from heat curing are thought to be effective in this process. It has also been determined that the matrix is quite dense. Figure 15b shows the microstructure images of the Mix4 mixture hardened in the ambient. This mix has the lowest compressive strength at 24.5 MPa. Thorny CSH gels in cementitious systems were observed rather than spherical CSH gels in the matrix. Despite the ambient curing of the mixtures, CSH gels were formed. CASH gels were also observed in the matrix. Dense CSH gels were observed due to the high GBFS and alkaline solution content. Withal, non-hydrated GBFS particles were observed in the mixtures treated with ambient curing. Geopolymerization slowed down as the ambient curing was about 22 °C. As a result, non-hydrated GBFS particles led to a decrease in compressive strength. The non-hydrated GBFS particles acted as fillers. Additionally, the matrix contains a network of microcracks. In general, in both SEM images, it was observed that the microstructure has been observed to be dense, compact, and homogeneous.

Figure 16a shows the microstructure of the Mix1 mixture exposed to 800 °C at different magnifications. Mapping cracks were noticed in some areas of the matrix. It was determined that these cracks were formed during the heat-curing process rather than at a high temperature. In other words, these mapping cracks are mostly formed due to drying shrinkage. However, microcracks were frequently observed in the crack width range of 1–10 µm. The effect of

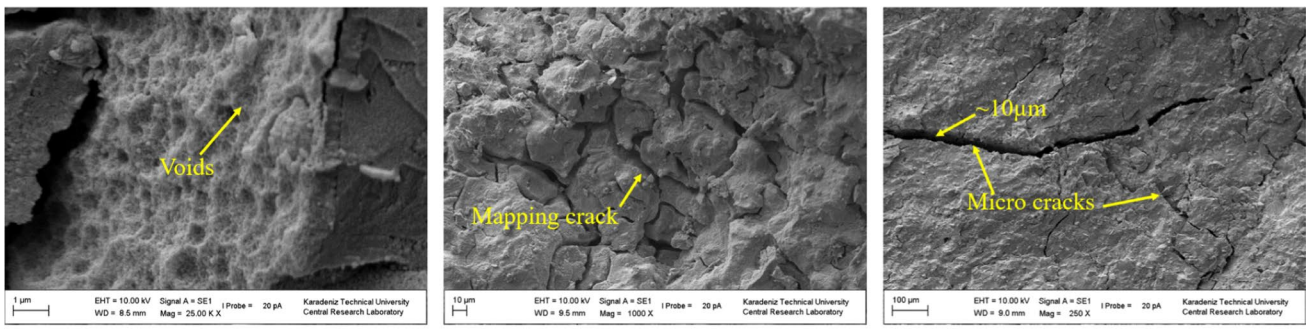


(a) Mix 1 (Cured at 75°C)

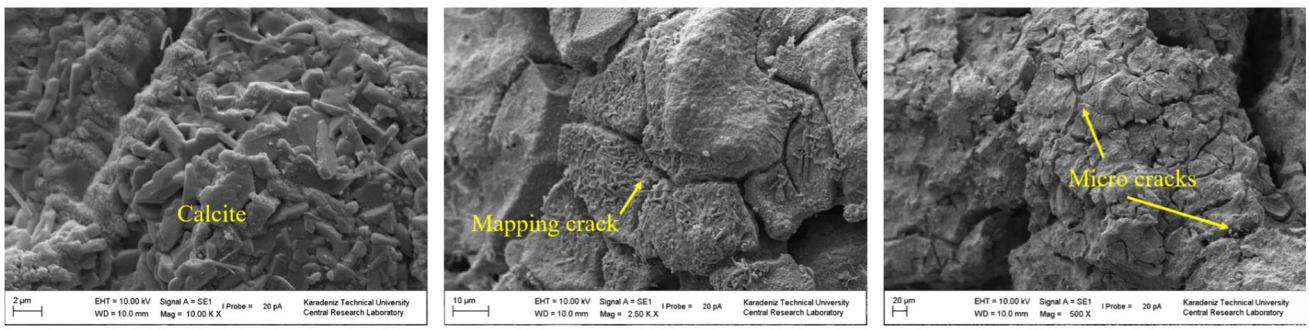


(b) Mix 4 (Cured at ambient temperature)

Fig. 15 Microstructures of ambient and heat-cured mixtures. **a** Mix1 mixture exposed to 800 °C (cured at 75 °C). **b** Mix4 mixture exposed to 800 °C (cured at ambient temperature)



(a) Mix1 mixture exposed to 800°C (Cured at 75°C)



(b) Mix4 mixture exposed to 800°C (Cured at ambient temperature)

Fig. 16 Microstructures of the mixtures exposed to high-temperature

elevated temperature formed these cracks. The compressive strength of the Mix1 sample decreased by approximately 85% after 800 °C. A dense CSH gel was determined in the matrix due to the high GGBFS and alkaline activator. Nevertheless, since these gels formed after 800 °C were severely damaged, the rate of strength loss was quite high. In fact, it has been observed that voids are formed in the regions where these gels disappear. Microscopic air voids were found in the M1 mixture that was cured at 75 °C for 8 h. Similar images were also detected in Fig. 16b of the Mix4 mixture. In addition, calcite crystals were determined in the matrix of the Mix4 mixture. Since calcite crystals are generally damaged at 900 °C, these crystals have been determined in some regions. Calcite is formed from the hydration of C_2S within GGBFS. Because C_2S forms Portlandite during hydration. As a result of the carbonation of Portlandite, calcite crystals in SEM images were formed. Since the geopolymerization products decomposed at 800 °C, the porosity increased. A slight increase in strength was determined at 200 °C due to the abundance of non-hydrated particles in the Mix4 mixture. Thanks to this effect, the compressive strength of the Mix4 sample decreased by 51% after 800 °C. As a result, the binder and alkali solution content should be considered in the design of geopolymer composites subject to high-temperature effects. The excess gels formed increase the damage under the effect of elevated temperatures, such as 800 °C.

5 Statistical evaluations

In the current study, the multi-factor analysis of variance (ANOVA) was used to statistically evaluate the experimental results achieved. The analysis was performed to examine the effectiveness of the independent parameters like No.5 CA fraction, curing regime strategies, and/or elevated-temperature exposure on the investigated physical properties and strength characteristics. Herein, the MINITAB named software was employed in performing the statistical analysis. The evaluated results are presented in Table 5. The observations implied that all physical properties of AAC mixtures were affected by No.5 CA weight fraction and curing regime at changing contributions. However, the curing regime with a contribution of more than about 60% was the most significant experimental parameter affecting the physical properties of AAC mixtures. Similarly, the No.5 CA weight fraction and the curing regime have a significant influence on the flexural strength of the AAC mixtures, and the curing regime with a contribution of about 79% has exerted more than the No.5 CA weight fraction. Withal, since the impact of high temperature on the compressive strength and mass loss was also inspected in the current study, its statistical impact was also evaluated. It was seen that all experimental parameters influenced the mass loss of AAC mixtures whereas it was seen that the No.5 CA weight fraction is not a statistically important parameter of the compressive strength. Among the inspected parameters, the elevated temperature with the highest contribution value was the most significant parameter.

In addition to the multi-factor analysis of variance (ANOVA), the Pearson correlation matrix was constructed to determine the degree of correlation between each design parameter and experimental results. The correlation matrix constructed in this regard is displayed in Fig. 17. The correlation matrix will be interpreted based on the correlation coefficient value, which indicates the strength of the correlation. The coefficients range from 0 to 0.3 (bad), 0.3 to 0.5 (weak), 0.5 to 0.7 (moderate), 0.7 to 0.9 (good), and 0.9 to 1.0 (high).

Correlation between the curing regime and experimental results:

- Positive association with unit weight, 8-h compressive strength, and 8-h flexural strength with a good coefficient of correlation (see Fig. 17).
- Negative association with water absorption, apparent porosity, and capillary water absorption with a good coefficient of correlation (see Fig. 17).

Correlation between the No.5 CR fraction and experimental results:

- Positive association with water absorption and capillary water absorption with a weak coefficient of correlation, and apparent porosity with a moderate coefficient of correlation (see Fig. 17).
- Negative association with unit weight, 8-h compressive strength, and 8-h flexural strength with a weak coefficient of correlation (see Fig. 17).

Moreover, Fig. 17 can be investigated in detail to see the association among the experimental results.

6 Conclusions

The following conclusions can be taken from the current study:

– Increasing the fraction of CA No.5 in the ACC resulted in more flowable AAC mixtures. The difference in fineness moduli between No.10 and No.5 CAs, along with the lower water absorption capacity of No.5 CA, contributes to this increase.
– Consistently substituting No10 CA with No5 type reduces the unit weights of ACC mixtures under all cur-

Table 5 Statistical evaluation of the experimental results

Investigated parameter	Experimental parameter	Degree of freedom	The sequential sum of squares	Computed F	Significance (*P* value)	Contribution (%)
Unit weight	No.5 CA fraction	3	6424.9	13.61	YES (<0.05)	25.7
	Curing regime	2	17,643.5	56.08	YES (<0.05)	70.5
	Error	6	943.8	–	–	3.8
	Total	11	25,012.2	–	–	–
Apparent porosity	No.5 CA fraction	3	8.4587	6.34	YES (<0.05)	30.6
	Curing regime	2	16.5004	18.56	YES (<0.05)	59.7
	Error	6	2.6673	–	–	9.7
	Total	11	27.6264	–	–	–
Water absorption	No.5 CA fraction	3	15.155	7.41	YES (<0.05)	25.1
	Curing regime	2	41.157	30.18	YES (<0.05)	68.1
	Error	6	4.091	–	–	6.8
	Total	11	60.402	–	–	–
Capillary water absorption	No.5 CA fraction	3	0.15617	5.09	YES (<0.05)	18.0
	Curing regime	2	0.64902	31.72	YES (<0.05)	74.9
	Error	6	0.06138	–	–	7.1
	Total	11	0.86657	–	–	–
Flexural strength	No.5 CA fraction	3	1.0074	16.54	YES (<0.05)	18.9
	Curing regime	2	4.2134	103.73	YES (<0.05)	78.9
	Error	6	0.1218	–	–	2.3
	Total	11	5.3426	–	–	–
Compressive strength	No.5 CA fraction	3	166.4	1.20	NO (>0.05)	1.4
	Curing regime	2	1197.3	12.95	YES (<0.05)	10.4
	Elevated temperature	3	8332.9	60.09	YES (<0.05)	72.5
	Error	39	1802.8	–	–	15.7
	Total	47	11,499.4	–	–	–
Weight loss	No.5 CA fraction	3	4.271	10.15	YES (<0.05)	0.8
	Curing regime	2	3.905	13.92	YES (<0.05)	0.7
	Elevated temperature	2	536.426	1912.13	YES (<0.05)	97.8
	Error	28	3.928	–	–	0.7
	Total	35	548.529	–	–	–

ing strategies. The main reason for this scenario is the relatively lower specific gravity of No.5 CA.

- Heat curing increased the unit weight due to the accelerated geopolymerization reaction at higher temperatures.
- Increasing the No.5 CA weight fraction increased apparent porosity caused by the gradation of fine aggregate. The heat-curing process resulted in a lower porosity in the mixtures due to the geopolymerization reaction occurring at a faster rate with increasing temperature.
- Increasing the fraction of CA No.5 improves the absorption capacities regardless of the curing strategy type. However, heat curing applied to the AAC mixtures enhances their water absorption performances.
- Increasing the weight fraction of No.5 CA systematically decreases the 8-h flexural and compressive strengths. Increasing aggregate size reduces strength performance due to larger aggregate-paste interfaces.
- Raising the curing temperature during heat treatment enhanced both the 8-h flexural and compressive strengths. Heat curing enhances geopolymerization, resulting in a significant increase in strength performance.
- Exposure to high temperatures caused a significant amount of mass loss and a significant decrease in the compressive strengths of the AAC mixes. The AAC mixes cured with heat outperformed when exposed to high temperatures.
- Curing the AAC mixtures at a higher temperature will increase the fire resistance.
- At all elevated temperatures, increasing the weight fraction of CA No.5 resulted in higher residual compressive strength values with confidence. The weight fraction of CA No.5 did not significantly affect mass loss, especially at higher temperature exposures.

Variables	CR	No5CA	WA	AP	UW	CWA	CompStr	FlexStr
CR	1	0.000	-0.814	-0.738	0.757	-0.799	0.880	0.888
No5CA	0.000	1	0.459	0.510	-0.486	0.394	-0.415	-0.429
WA	-0.814	0.459	1	0.978	-0.964	0.951	-0.968	-0.909
AP	-0.738	0.510	0.978	1	-0.968	0.972	-0.934	-0.854
UW	0.757	-0.486	-0.964	-0.968	1	-0.973	0.951	0.873
CWA	-0.799	0.394	0.951	0.972	-0.973	1	-0.945	-0.867
CompStr	0.880	-0.415	-0.968	-0.934	0.951	-0.945	1	0.969
FlexStr	0.888	-0.429	-0.909	-0.854	0.873	-0.867	0.969	1

CR: Curing regime; **No5CA**: No.5 CA fraction; **WA**: Water absorption; **AP**: Apparent porosity; **UW**: Unit weight; **CWA**: Capillary water absorption; **CompStr**: 8-hour compressive strength; **FlexStr**: 8-hour flexural strength

Fig. 17 Pearson correlation matrix of the specified design parameters and experimental results

- Using a higher amount of CA No.5 will increase the fire resistance.
- The curing temperature applied to AAC mixtures has a significant impact on their engineering features and microstructural characteristics. It has an important effect on the performance of such composites as much as their compositions.

7 Recommendations for future works

The authors strongly recommend that researchers include Energy Dispersive X-ray spectroscopy (EDX) elemental mapping or spot analysis data to support the interpretations of the SEM images. This is because EDX analysis can validate the composition and elemental distribution of the observed phases and products, such as C–S–H gels. By doing so, the researchers can confidently assert the accuracy of their findings and conclusions.

Funding Open access funding provided by the Scientific and Technological Research Council of Türkiye (TÜBİTAK). This study was not funded by any supporter.

Data availability Some or all data presented in the current study can be provided by request.

Declarations

Conflicts of interest The authors declare that they have no known competing financial interests or personal relationships that could have appeared to influence the work reported in the paper.

Human and animals rights statement The study does not involve human and animals.

Informed consent The study does not require an informed consent.

Open Access This article is licensed under a Creative Commons Attribution 4.0 International License, which permits use, sharing, adaptation, distribution and reproduction in any medium or format, as long as you give appropriate credit to the original author(s) and the source, provide a link to the Creative Commons licence, and indicate if changes were made. The images or other third party material in this article are included in the article's Creative Commons licence, unless indicated otherwise in a credit line to the material. If material is not included in the article's Creative Commons licence and your intended use is not permitted by statutory regulation or exceeds the permitted use, you will need to obtain permission directly from the copyright holder. To view a copy of this licence, visit http://creativecommons.org/licenses/by/4.0/.

References

1. Andrew RM. Global CO_2 emissions from cement production, 1928–2018. Earth Syst Sci Data. 2019;11(4):1675–710. https://doi.org/10.5194/essd-11-1675-2019.
2. Argiz C, Sanjuan MA, Munoz-Martialay R. Effect of the aggregate grading on the concrete air permeability. Mater Constr. 2014;64(315): e026. https://doi.org/10.3989/mc.2014.07213.
3. Ashraf WB, Noor MA. Effects of aggregate gradation on water permeability of concrete. Adv Mater Res. 2012;488–489:248–52. https://doi.org/10.4028/www.scientific.net/AMR.488-489.248.
4. ASTM C138/C138M-17a. Standard test method for density (unit weight), yield, and air content (Gravimetric) of concrete. ASTM International, West Conshohocken, PA. 2017. https://doi.org/10.1520/C0138_C0138M-17A
5. ASTM C1437-20. Standard test method for flow of hydraulic cement mortar. ASTM International, West Conshohocken, PA. 2020. https://doi.org/10.1520/C1437-20
6. ASTM C348-20. Standard test method for flexural strength of hydraulic-cement mortars. ASTM International, West Conshohocken, PA. 2020. https://doi.org/10.1520/C0348-20
7. ASTM C349-18. Standard test method for compressive strength of hydraulic-cement mortars (using portions of prisms broken in flexure). ASTM International, West Conshohocken, PA. 2018. https://doi.org/10.1520/C0349-18
8. ASTM C642-21. Standard test method for density, absorption, and voids in hardened concrete. ASTM International, West Conshohocken, PA. 2021. https://doi.org/10.1520/C0642-21
9. ASTM C989/C989M-18a. Standard specification for slag cement for use in concrete and mortars. ASTM International, West Conshohocken, PA. 2018. https://doi.org/10.1520/C0989_C0989M-18A
10. Aydin S. A ternary optimisation of mineral additives of alkali activated cement mortars. Constr Build Mater. 2013;43:131–8. https://doi.org/10.1016/j.conbuildmat.2013.02.005.

11. Aydin S, Baradan B. Efect of activator type and content on properties of alkali-activated slag mortars. Compos B. 2014;57:166–72. https://doi.org/10.1016/j.compositesb.2013.10.001.
12. Basheer L, Basheer PAM, Long AE. Influence of coarse aggregate on the permeation, durability and the microstructure characteristics of ordinary Portland cement concrete. Constr Build Mater. 2005;19(9):682–90. https://doi.org/10.1016/j.conbuildmat.2005.02.022.
13. Bayrak B, Öz A, Benli A, Kavaz E, Kaplan G, Aydın AC. Physico-mechanical and shielding properties of alkali-activated slag composites incorporating cement clinker aggregate: Effect of high temperature and particle size. J Build Eng. 2023;67: 105982. https://doi.org/10.1016/j.jobe.2023.105982.
14. Berger RL. Properties of concrete with cement clinker aggregate. Cem Concr Res. 1974;4(1):99–112. https://doi.org/10.1016/0008-8846(74)90069-6.
15. Bing-hui M, Zhu H, Xue-min C, Yan H, Si-yu G. Effect of curing temperature on geopolymerization of metakaolin-based geopolymers. Appl Clay Sci. 2014;99:144–8. https://doi.org/10.1016/j.clay.2014.06.024.
16. BS EN 1015-18 (2002) Methods of test for mortar for masonry - determination of water absorption coefficient due to capillary action of hardened mortar. British Standards Institution, London, UK.
17. Carabba L, Moricone R, Scarponi GE, Tugnoli A, Bignozzi MC. Alkali activated lightweight mortars for passive fire protection: a preliminary study. Constr Build Mater. 2019;195:75–84. https://doi.org/10.1016/j.conbuildmat.2018.11.005.
18. Chithambaram SJ, Kumar S, Prasad MM. Thermo-mechanical characteristics of geopolymer mortar. Constr Build Mater. 2019;213:100–8. https://doi.org/10.1016/j.conbuildmat.2019.04.051.
19. CIP 16. 2016. Flexural strength of concrete. National Ready Mixed Concrete Association. www.nrmca.com
20. Ekmen Ş, Mermerdaş K, Algın Z. Effect of oxide composition and ingredient proportions on the rheological and mechanical properties of geopolymer mortar incorporating pumice aggregate. J Build Eng. 2021;34: 101893. https://doi.org/10.1016/j.jobe.2020.101893.
21. Gagg CR. Cement and concrete as an engineering material: an historic appraisal and case study analysis. Eng Fail Anal. 2014;40:114–40. https://doi.org/10.1016/j.engfailanal.2014.02.004.
22. Gao T, Shen L, Shen M, Chen F, Liu L, Gao L. Analysis on differences of carbon dioxide emission from cement production and their major determinants. J Clean Prod. 2015;103:160–70. https://doi.org/10.1016/j.jclepro.2014.11.026.
23. Gismera S, Alonso MD, Palacios M, Puertas F. Rheology of alkali-activated mortars: influence of particle size and nature of aggregates. Minerals. 2020;10(8):726. https://doi.org/10.3390/min10080726.
24. Hardjito D, Wallah SE, Sumajouw DMJ, Rangan BV. Factors influencing the compressive strength of fly ash-based geopolymer concrete. Civil Eng Dimen. 2004;6(2):88–93. https://doi.org/10.9744/ced.6.2.pp.88-93.
25. Huntzinger DN, Eatmon TD. A life-cycle assessment of Portland cement manufacturing: comparing the traditional process with alternative technologies. J Clean Prod. 2009;17(7):668–75. https://doi.org/10.1016/j.jclepro.2008.04.007.
26. İpek S. Macro and micro characteristics of eco-friendly fly ash-based geopolymer composites made of different types of recycled sand. J Build Eng. 2022;52: 104431. https://doi.org/10.1016/j.jobe.2022.104431.
27. Kaplan G, Öz A, Bayrak B, Alcan HG, Çelebi O, Aydın AC. The effect of curing temperature on the early age properties of granulated furnace slag based reactive geopolymer concrete. First International Geopolymeric Composites Congress (GEC-2021), 2021;29–30 December, Erzurum, Turkey.
28. Kovalchuk G, Fernandez-Jimenez A, Palomo A. Alkali-activated fly ash: effect of thermal curing conditions on mechanical and microstructural development - Part II. Fuel. 2007;86(3):315–22. https://doi.org/10.1016/j.fuel.2006.07.010.
29. Kürklü G. The efect of high temperature on the design of blast furnace slag and coarse fy ash-based geopolymer mortar. Compos B Eng. 2016;92:9–18. https://doi.org/10.1016/j.compositesb.2016.02.043.
30. Lee BY, Cho CG, Lim HJ, Song JK, Yang KH, Li VC. Strain hardening fiber-reinforced alkali-activated mortar - a feasibility study. Constr Build Mater. 2012;37:15–20. https://doi.org/10.1016/j.conbuildmat.2012.06.007.
31. Li H, Gao P, Xu F, Sun T, Zhou Y, Zhu J, Peng C, Lin J. Effect of fine aggregate particle characteristics on mechanical properties of fly ash-based geopolymer mortar. Minerals. 2021;11(8):897. https://doi.org/10.3390/min11080897.
32. Li YL, Zhao XL, Singh Raman RK, Al-Saadi S. Thermal and mechanical properties of alkali-activated slag paste, mortar and concrete utilising seawater and sea sand. Constr Build Mater. 2018;159:704–24. https://doi.org/10.1016/j.conbuildmat.2017.10.104.
33. Li Z, Liu S. Influence of slag as additive on compressive strength of fly ash-based geopolymer. J Mater Civ Eng. 2007;19(6):470–4. https://doi.org/10.1061/(ASCE)0899-1561(2007)19:6(470).
34. Mermerdaş K, İpek S, Mahmood Z. Visual inspection and mechanical testing of fly ash-based fibrous geopolymer composites under freeze-thaw cycles. Constr Build Mater. 2021;283:122756. https://doi.org/10.1016/j.conbuildmat.2021.122756.
35. Mermerdaş K, Manguri S, Nassani DE, Oleiwi SM. Effect of aggregate properties on the mechanical and absorption characteristics of geopolymer mortar. Eng Sci Technol. 2017;20(6):1642–52. https://doi.org/10.1016/j.jestch.2017.11.009.
36. Mohseni E, Kazemi MJ, Koushkbaghi M, Zehtab B, Behforouz B. Evaluation of mechanical and durability properties of fiber-reinforced lightweight geopolymer composites based on rice husk ash and nanoalumina. Constr Build Mater. 2019;209:532–40. https://doi.org/10.1016/j.conbuildmat.2019.03.067.
37. Nagral MR, Ostwal T, Chitawadagi MV. Effect of curing temperature and curing hours on the properties of geopolymer concrete. Int J Comput Eng Res. 2014;4(9). http://www.ijceronline.com/papers/Vol4_issue09/A039101011.pdf
38. Noushini A, Castel A. The effect of heat-curing on transport properties of low-calcium fly ash-based geopolymer concrete. Constr Build Mater. 2016;112:464–77. https://doi.org/10.1016/j.conbuildmat.2016.02.210.
39. Park R. (2003) Concrete, reinforced. In: Encyclopedia of physical science and technology. 3rd ed. Cambridge: Academic Press. 2003; p. 583–602. https://doi.org/10.1016/B0-12-227410-5/00134-4
40. Rangan BV. (2008) Fly ash-based geopolymer concrete. Research Report GC4, Engineering Faculty, Curtin University, Perth, Australia. 1999. https://espace.curtin.edu.au/bitstream/handle/20.500.11937/20680/20465_downloaded_stream_453.pdf?sequence=2&isAllowed=y. Accessed 02 Feb 2023.
41. Rovnanik P, Bayer P, Rovnanikova P. Characterization of alkali activated slag paste after exposure to high temperatures. Constr Build Mater. 2013;47:1479–87. https://doi.org/10.1016/j.conbuildmat.2013.06.070.
42. Rovnanik P, Safrankova K. Thermal behaviour of metakaolin/fly ash geopolymers with chamotte aggregate. Materials. 2016;9(7):535. https://doi.org/10.3390/ma9070535.
43. Rovnanik P. Effect of curing temperature on the development of hard structure of metakaolin-based geopolymer. Constr Build

Mater. 2010;24:1176–83. https://doi.org/10.1016/j.conbuildmat.2009.12.023.
44. Sajan P, Jiang T, Lau CK, Tan G, Ng K. Combined effect of curing temperature, curing period and alkaline concentration on the mechanical properties of fly ash-based geopolymer. Cleaner Mater. 2021;1: 100002. https://doi.org/10.1016/j.clema.2021.100002.
45. Shafaghat J, Allahverdi A. Using PC clinker as aggregate-enhancing concrete properties by improving ITZ microstructure. Mag Concr Res. 2020;72(4):173–81. https://doi.org/10.1680/jmacr.18.00134.
46. Turner LK, Collins FG. Carbon dioxide equivalent (CO_2-e) emissions: a comparison between geopolymer and OPC cement concrete. Constr Build Mater. 2013;43:125–30. https://doi.org/10.1016/j.conbuildmat.2013.01.023.
47. Xu ZK, Yue JC, Pang GH, Li RX, Zhang P, Xu ST. Influence of the activator concentration and solid/liquid ratio on the strength and shrinkage characteristics of alkali-activated slag geopolymer pastes. Adv Civil Eng. 2021;2021:1–11. https://doi.org/10.1155/2021/6631316.
48. Zhang J, Liu G, Chen B, Song D, Qi J, Liu X. Analysis of CO_2 emission for the cement manufacturing with alternative raw materials: a LCA-based framework. Energy Procedia. 2014;61:2541–5. https://doi.org/10.1016/j.egypro.2014.12.041.
49. Zhang H, Li L, Yuan C, Wang Q, Sarker PK, Shi X. Deterioration of ambient-cured and heat-cured fly ash geopolymer concrete by high temperature exposure and prediction of its residual compressive strength. Constr Build Mater. 2020;262: 120924. https://doi.org/10.1016/j.conbuildmat.2020.120924.

Publisher's Note Springer Nature remains neutral with regard to jurisdictional claims in published maps and institutional affiliations.